Synthetic Aperture Radar Imaging Using a Unique Approach to Frequency-Modulated Continuous-Wave Radar Design

Gregory L. Charvat and Leo C. Kempel

Department of Electrical and Computer Engineering
Michigan State University
2120 Engineering Building, East Lansing, MI 48825 USA
E-mail: charvatg@msu.edu, kempel@egr.msu.edu

Abstract

Synthetic-aperture-radar (SAR) imaging is an expensive endeavor. It can be difficult for universities, small business, or individuals to experiment with SAR imaging and algorithm development on a low budget. For this reason, a uniquely inexpensive solution to frequency-modulated continuous-wave (FMCW) radar was developed and then utilized as an ultra-low-cost SAR imaging system. This unique approach to FMCW radar used a pair of low-cost Gunn-oscillator-based microwave transceiver modules, known as "Gunnplexers." These transceiver modules had stability and noise problems, causing them to be unsuitable for use in precise FMCW radar applications when just one module was used. In order to overcome this problem, a unique radar solution was developed that used a combination of two transceiver modules to create a precise and inexpensive FMCW radar system, capable of producing SAR imagery on a budget.

Keywords: FM radar; CW radar; Gunn device oscillators; synthetic aperture radar; radar Imaging; radar equipment

1. Introduction

The objective of this article is to prove that synthetic-aperture radar (SAR) imaging on an extremely low budget is possible. This research was conducted by the Michigan State University Electromagnetics Research Group in an effort to expand our research opportunities at a minimum financial risk. A unique approach to frequency-modulated continuous-wave (FMCW) radar design was developed and utilized as an ultra-low-cost SAR imaging system. This system was then used successfully to develop four different SAR imaging algorithms, which have been used in a number of subsequent research projects.

The unique approach to FMCW was previously introduced in [1, 2], and [3]. Section 2 is an explanation of the MA87127-1 Gunn-oscillator-based transceiver module, known as a "Gunnplexer." An explanation of the unique approach to FMCW radar is presented in Section 3. Range profile results are presented in Section 4. Section 5 explains the SAR system implementation. Section 6 presents imaging results using a range-stacking SAR algorithm. Section 7 presents imaging results using two versions of the polar-format algorithm (PFA). Section 8 presents imaging results using the range-migration algorithm (RMA). Conclusions and future work are discussed in Section 9.

2. The MA87127-1 Transceiver Module

The unique approach to FMCW radar design depends on the use of two inexpensive microwave transceiver modules. These modules are Gunn-diode based, and are more commonly known as "Gunnplexers." The particular microwave transceiver module used for this system is the M/A-Com model MA87127-1 X-band microwave transceiver module. In practice, almost any X-band varactor-tuned Gunnplexer could be used to implement this system.

The MA87127-1 is composed of three major components: a voltage-controlled oscillator (VCO), a mixer, and a circulator (see Figure 1). The VCO is fed into port 1 of the circulator. Port 2 of the circulator is connected to the WR-90 waveguide flange input/output port of the transceiver. Port 3 of the circulator is connected to the RF input of the mixer. Some power is coupled off the VCO and fed into the local-oscillator (LO) port of the mixer. The IF output of the mixer is connected to a small solder terminal on the outer case of the transceiver.

VCO1 is a varactor-controlled Gunn-diode oscillator. A varactor diode is placed inside of a cavity Gunn oscillator, as shown in Figure 2. A bias voltage on the varactor diode, between

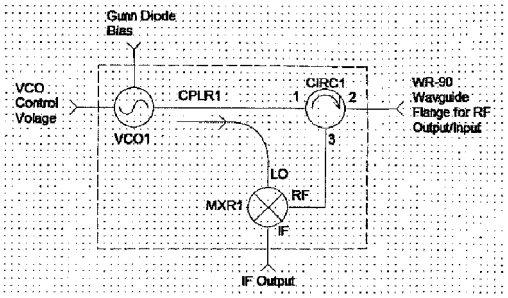

Figure 1. A block diagram of the MA87127-1.

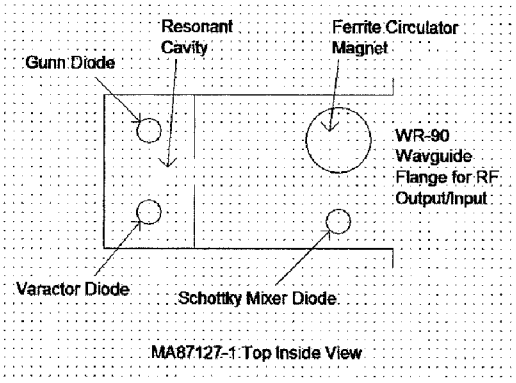

Figure 2. The physical layout of the MA87127-1.

roughly 0 and 20 V, controls the frequency of the Gunn oscillator. A second bias voltage, of approximately 10 V, causes the Gunn diode to oscillate at the frequency of the cavity in which it is placed.

Looking at Figure 1, CPLR1 is a symbolic representation of the coupling action that occurs between the Gunn-oscillator diode and the Schottky mixer diode placed within close proximity, as shown in Figure 2. MXR1 is created by the coupled power from the Gunn-diode oscillator. This coupled power causes the Schottky mixer diode to switch on and off. This switching action causes the Schottky mixer diode to operate as a single balanced mixer.

CIRC1 is a ferrite circulator, placed inside of the WR90 waveguide that contains MXR1 and that is weakly coupled to the resonant cavity where the Gunn oscillator is located. CIRC1 is basically a large magnet, precisely placed inside of the WR90 waveguide section. CIRC1 causes RF power from VCO1 to exit the input/output port, and causes RF power coming into the input/output port to be transferred into MXR1.

When looking at Figure 1, it appears as though just one transceiver module alone can be utilized as an FMCW radar system. However, it was found in lab tests that the pass band of the IF port on MXR1 started to roll off around 1 MHz, causing little to no response at audio frequencies, which is were most beats from a short-range FMCW radar system will be located. The transceiver module's receiver worked most efficiently at IF frequencies above 30 MHz, where the loss due to the mixer was found to be the least. The lack of an acceptable low-frequency-to-near-dc response from MXR1 renders one individual transceiver module useless for most short-range FMCW radar applications.

Regardless of its shortcomings, when two MA87127-1 (or similar) transceiver modules are used together, the unique FMCW radar design solution can be obtained.

3. The Unique Approach to FMCW Radar

In order to fully understand the unique approach to FMCW radar, the reader must be well versed in the theoretical operation of FMCW radar systems. A good explanation of FMCW radar can be found in [4]. The unique approach to FMCW radar was implemented using two low-cost MA87127-1 Gunn-diode-based transceiver modules. All schematics and further explanation of this design can be found in [1]. A picture of the system is shown in Figure 3. Figure 4 shows a simplified block diagram of the FMCW radar system.

The following is a mathematical explanation of the unique approach to FMCW radar. The MA87127-1 transceiver module XCVR1 is centered at frequency f_1 and FM modulated with a linear chirp, kf_d, where $k = \frac{\text{volts}}{\text{second}}$. The output of XCVR1 is represented by the equation

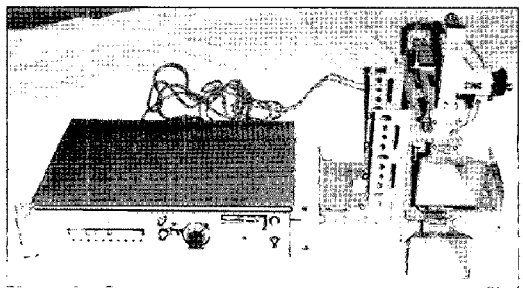

Figure 3. A unique approach to FMCW radar.

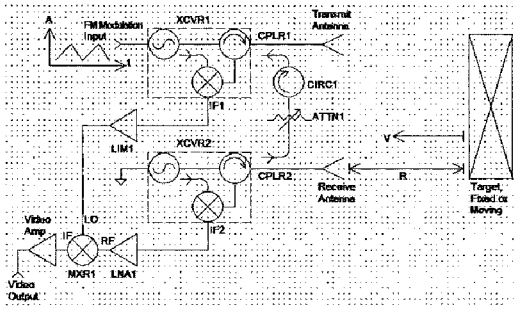

Figure 4. A simplified block diagram of the unique FMCW radar solution.

$$TX_1(t) = \cos(2\pi f_1 t + 2\pi k f_d). \quad (1)$$

The output of XCVR1 is fed into the transmitting antenna. The transmitted signal is radiated out toward the target scene, and then reflected off of the target. The target is situated at a range, R, and moving at a velocity, v (if it is moving). The range, R, and velocity, v, correspond to a time difference and Doppler shift between the original transmitted signal, and that which was picked up by the receiving antenna and fed into the MA87127-1 transceiver module, XCVR2. This time difference corresponds to a beat-frequency difference f_b, as shown in [4]. Thus, the reflected signal from the target is represented by the equation

$$TX_{1b}(t) = \cos(2\pi f_1 t + 2\pi k f_d + 2\pi f_b t). \quad (2)$$

XCVR2 is set to a fixed frequency of f_2. XCVR2 is radiating a fixed-frequency carrier at that frequency, which can be represented by the equation

$$TX_2(t) = \cos(2\pi f_2 t). \quad (3)$$

As explained in Section 2, the IF output of each transceiver module is the product of its VCO frequency and any RF power that is coming into the input/output port of the module. Because of this, the IF output of XCVR2 can be calculated to be

$$\begin{aligned} IF_2(t) &= TX_{1b}(t)TX_2(t) \\ &= \frac{1}{2}\cos(2\pi f_1 t + 2\pi k f_d t + 2\pi f_b t + 2\pi f_2 t) \\ &+ \frac{1}{2}\cos(2\pi f_1 t + 2\pi k f_d t + 2\pi f_b t - 2\pi f_2 t). \end{aligned} \quad (4)$$

The higher-frequency term can be dropped. This is a practical consideration, since the IF output ports of the transceiver modules are not capable of producing X-band microwave signals. Thus, the IF output of XCVR2 can be simplified to

$$IF_2(t) = \frac{1}{2}\cos(2\pi f_1 t + 2\pi k f_d t + 2\pi f_b t - 2\pi f_2 t). \quad (5)$$

Simultaneously, some power from XCVR2 is coupled into XCVR1, taking advantage of a coupling problem that would otherwise limit a typical FMCW radar system. Power from XCVR2 is deliberately coupled out using CPLR2 and output through ATT1, CIRC1, and into CPLR1. The coupled power injected into CPLR1 is fed into XCVR1. The resulting frequency response at the IF port of XCVR1 is calculated using the equation

$$\begin{aligned} IF_1(t) &= TX_2(t)TX_1(t) \\ &= \frac{1}{2}\cos(2\pi f_2 t + 2\pi f_1 t + 2\pi k f_d t) \\ &+ \frac{1}{2}\cos(2\pi f_2 t - 2\pi f_1 t - 2\pi k f_d t). \end{aligned} \quad (6)$$

Like XCVR2, the higher-frequency term can be dropped. Thus, the IF output of XCVR1 can be simplified to

$$IF_1(t) = \frac{1}{2}\cos(2\pi f_2 t - 2\pi f_1 t - 2\pi k f_d t). \quad (7)$$

$IF_1(t)$ is fed into the input port of a limiting amplifier, LIM1. The output of LIM1 is used as the LO drive of MXR1. $IF_2(t)$ is fed into the input port of a low-noise amplifier (LNA), which is represented by LNA1. The output of LNA1 is fed into the RF input port of MXR1. $IF_1(t)$ and $IF_2(t)$ are multiplied together in MXR1. The IF output of MXR1 is amplified by a video amplifier. The resulting product from MXR1 can be represented by the equation

$$\text{Video Output} = IF_1(t)IF_2(t). \quad (8)$$

The IF port of MXR1 is not capable of reproducing the high-frequency terms resulting from the multiplication of two sinusoidal signals. Therefore, the video output of the radar system can be expressed as

$$\text{Video Output} = \frac{1}{4}\cos(2\pi f_b t). \quad (9)$$

It is clear from the equation above that the video output is the beat-frequency difference, f_b, due to the distance from the target, R, and the velocity of the target, v. Thus, we have a homodyne FMCW radar system using two inexpensive microwave transceiver modules.

4. Range Profile Results

The unique approach to FMCW radar has the following specifications:

Center frequency = 10.25 GHz
Chirp bandwidth = 70 MHz
Transmit power = 10 dBm
Front end noise figure = 10 dB

Knowing these specifications, several range profiles were taken of standard radar targets, placed directly in front of the transmitting and receiving antennas at some range from the radar system. The range profiles were created by taking the discrete Fourier transform (DFT) of the digitized complex video data. Two range profiles are presented in this paper. Figure 5 is a range profile of a 30 dBsm

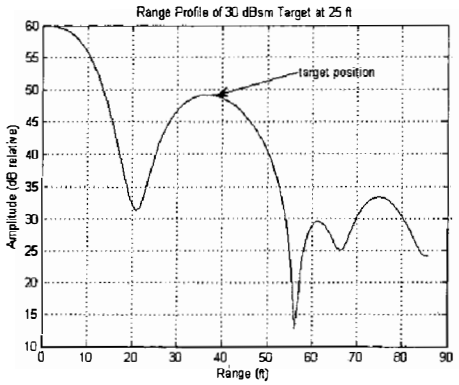

Figure 5. The range profile of a 30 dBsm trihedral corner reflector at a range of 25 ft.

trihedral corner reflector, placed at a range of 25 ft from the radar system. The position of the target is clearly visible in this range profile.

Figure 6 is a range profile of a 30 dBsm trihedral corner reflector placed at a range of 40 ft from the radar system. The position of the target is clearly visible in this range profile.

Looking at the range profiles shown in Figures 5 and 6, it is clear that there are some range-offset and nonlinear responses occurring. The constant range offset is due to internal hardware cable delays. This will not affect SAR imaging. The slight variation in linear ranging is due to the nonlinear tuning of the varactor-tuned Gunn oscillator. A tuning linearity plot of the MA87127-1 is shown in [1]. In general, varactor-tuned oscillators are not linear. However, this problem must be tolerated in order to operate such an inexpensive radar system.

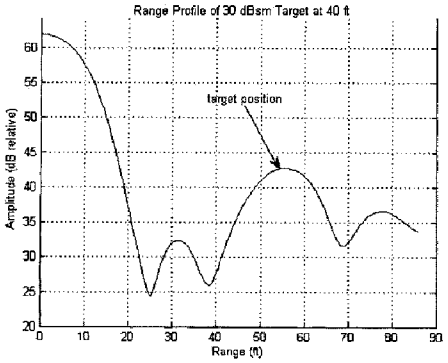

Figure 6. The range profile of a 30 dBsm trihedral corner reflector at a range of 40 ft.

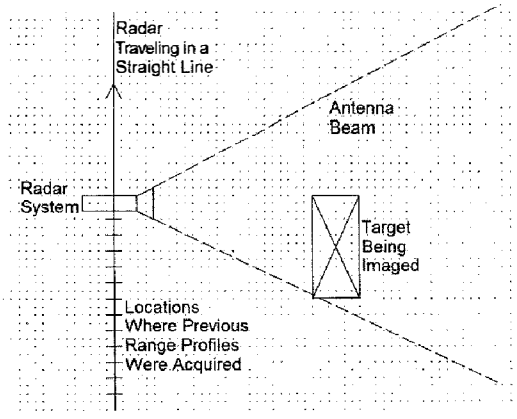

Figure 7. The experimental setup of the linear SAR imaging system.

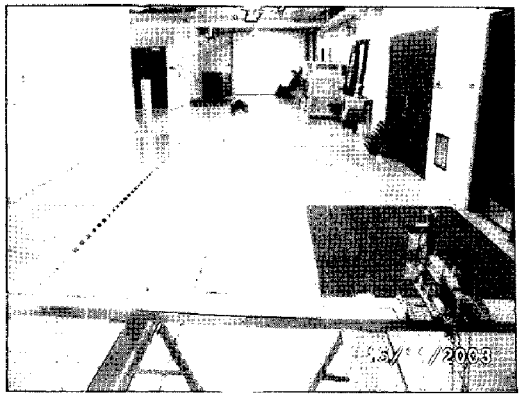

Figure 8. A picture of the rail SAR experimental setup. This particular experiment was performed indoors. Shown in the foreground is the linear SAR track, and in the background are two standard radar targets.

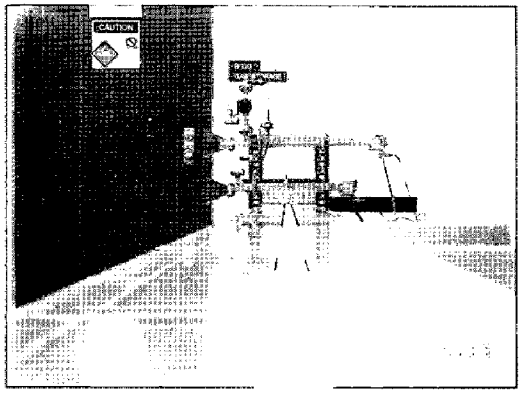

Figure 9. The front end of the unique approach to FMCW radar is moved along the linear SAR rail manually, where the user lines up the front-end chassis with a measuring tape laid down on the surface of the rail.

5. SAR System Implementation

A linear-rail SAR was implemented using the unique approach to FMCW radar. A diagram of this implementation is shown in Figure 7. The radar was mounted on a carrier that traversed a 12-foot-long linear rail. The transmitting and receiving antennas were directed away from and perpendicular to the track, towards the image scene. Range profiles were acquired at regular intervals as the radar traversed the rail. A picture of this setup is shown in Figure 8.

Data acquisition was performed using a National Instruments PCI6014 data acquisition card. A Labview VI was programmed to control data acquisitioning and some pre-processing. Data acquisition was triggered by two inputs. The first input resulted from the VI prompting the user to move the radar manually one inch down

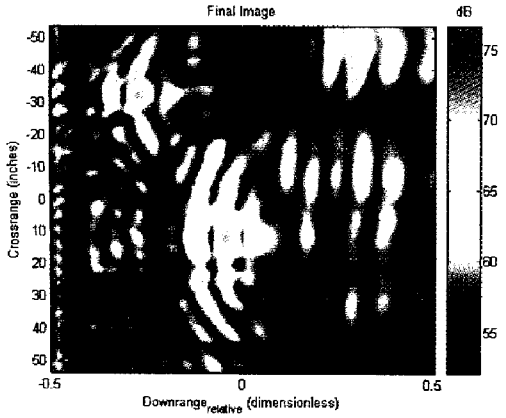

Figure 10. The SAR image formed using the range-stacking algorithm.

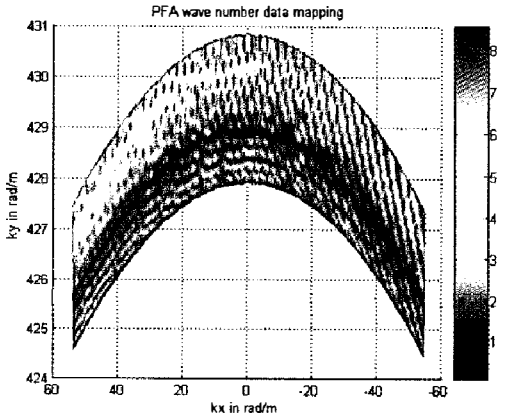

Figure 11. The polar-format algorithm wavenumber mapping of the SAR data; the real part of each data point is shown.

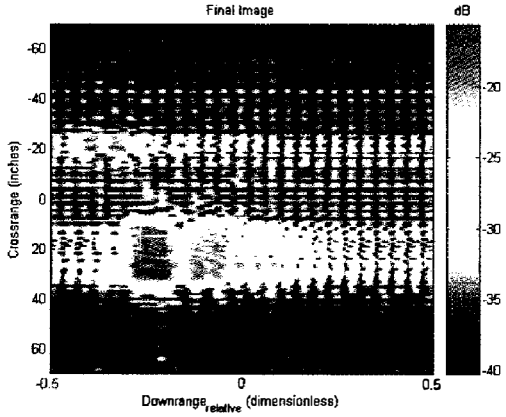

Figure 12. The SAR image formed using the polar-format algorithm with the narrow-beamwidth and narrow-bandwidth assumption.

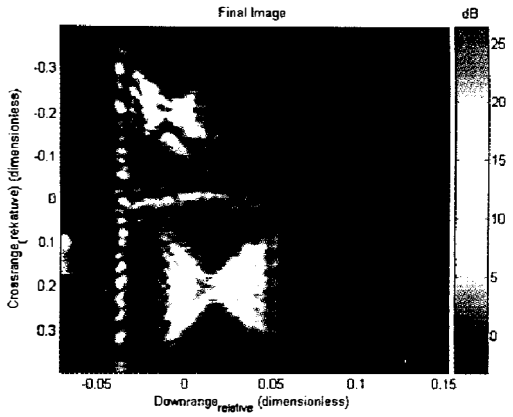

Figure 13. The SAR image formed using the polar-format algorithm.

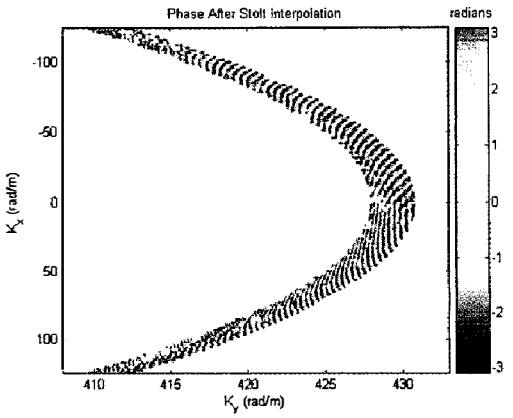

Figure 14. The range-migration algorithm wavenumber mapping of the SAR data; the phase of each data point is shown.

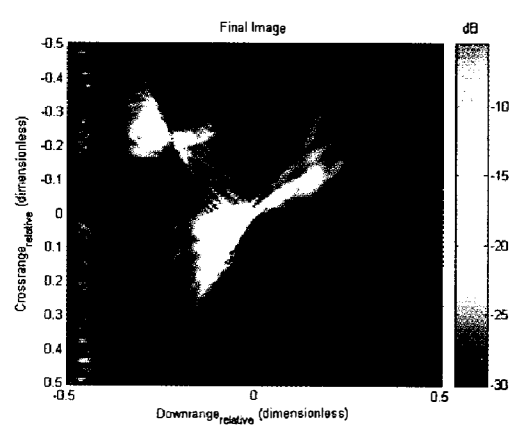

Figure 15. The SAR image formed using the range-migration algorithm.

the track. After the radar was moved one inch, the user hit enter. A significant cost-savings method used in implementing an ultra-low-cost SAR imaging system was moving the radar manually and lining up its position with a measuring tape (see Figure 9). The VI then waited for an external hardware trigger from a pulse generator. On the rising edge of this trigger, the data acquisition card simultaneously modulated the radar with a linear ramp and digitized the video output of the radar unit, storing the range profile in a two-dimensional data file. 2000 samples of the video output of the radar unit were digitized at a rate of 200 ksps. This process was performed every one inch, until the radar had traversed the entire 12-foot-long track. Real over-sampled video data was converted to complex I and Q data by use of the formula

$$S_{complex} = Video\_Output + jH\left(Video\_Output\right), \qquad (10)$$

where $H\left(Video\_Output\right)$ is the Hilbert transform, and $S_{complex}$ was decimated by two, throwing out every other sample.

This complex data was compiled into a two-dimensional matrix of radar position as a function of range profile. This data was used to create SAR imagery, using four different SAR algorithms.

6. Range-Stacking Algorithm

A range-stacking algorithm was implemented directly from [5]. In this experiment, a 20 dBsm trihedral corner reflector was placed 25 ft downrange from the rail, and a 30 dBsm trihedral corner reflector was placed 40 ft downrange from the rail. The targets were offset slightly from the center of the rail. The resulting image is shown in Figure 10. Looking at Figure 10, it is clear that the unique approach to FMCW radar in conjunction with a manually operated SAR rail was capable of producing detailed SAR using a range-stacking algorithm. However, it may be possible to create a more focused image using more advanced techniques.

7. The Polar-Format Algorithm

Two versions of the polar-format algorithm (PFA) were implemented directly from [6]. A target scene was set up with a 20 dBsm trihedral corner reflector located 25 ft from the rail, and a 30 dBsm trihedral corner reflector located 65 ft from the rail. The polar-format algorithm is based on matched filtering to scene center and nonlinear wavenumber mapping of the radar data. Once these tasks are performed, a two-dimensional discrete Fourier transform (DFT) is used to extract the image. Due to wavenumber mapping of the radar data, an interesting relationship occurred: the shorter the linear SAR rail, the greater the aperture bandwidth. Thus, the shorter the aperture bandwidth, the more curvy the wavenumber mapping of the radar data became. This relationship was explained in [6]. In the case of this particular system, the aperture length was an extremely short 12 ft. The scene center was located at 40 ft from the rail. The transmitter bandwidth was only 70 MHz, centered at 10.25 GHz. These factors contributed to a curved data mapping, which is shown in Figure 11.

One method of creating polar-format-algorithm SAR imagery from this data is to simply ignore the curvature and assume that the data is planar. This is known as the narrow-beamwidth and narrow-bandwidth assumption. The resulting image, using the narrow-beamwidth and narrow-bandwidth assumption, is shown in Figure 12. It is clear from Figure 12 that the image was extremely blurred and unclear. However, the polar-format algorithm with the narrow-bandwidth and narrow-beamwidth assumption is an extremely fast algorithm, requiring no interpolation. Thus, this algorithm is useful in creating a rough but fast image of a target scene.

A full polar-format algorithm was implemented. The polar-format algorithm utilizes a two-dimensional interpolation in the data-mapping phase of the algorithm. This takes time; however, it forms very detailed imagery. The resulting image using the polar-format algorithm is shown in Figure 13. Looking at Figure 13, it was clear that the unique approach to FMCW radar in conjunction with a manually operated SAR rail was capable of producing detailed SAR imagery using the polar-format algorithm.

8. The Range-Migration Algorithm

A range-migration algorithm was developed directly from [7]. A target scene was set up with a 20 dBsm trihedral corner reflector located 25 ft from the rail, and a 30 dBsm trihedral corner reflector located 65 ft from the rail. The range-migration algorithm is similar to the polar-format algorithm in that wavenumber data mapping is necessary. However, it differs greatly from the polar-format algorithm in that the range-migration algorithm's matched filter is a line, rather than a point in the scene center. This causes a dramatically different wavenumber mapping to occur, known as the Stolt interpolation. The Stolt interpolation compensates for geometric distortions in the resulting image due to wavefront curvature. The range-migration algorithm is faster than the polar-format algorithm, because the Stolt interpolation is only a one-dimensional interpolation. The wavenumber mapping for the range-migration algorithm using data collected by the unique approach to FMCW radar is shown in Figure 14.

After the Stolt interpolation, an inverse two-dimensional discrete Fourier transform process is performed on the data, which extracts the image. The resulting image formed using the range-migration algorithm is shown in Figure 15. Looking at Figure 15, it is clear that the unique approach to FMCW radar in conjunction with a manually operated SAR rail was capable of producing detailed SAR imagery using the range-migration algorithm.

6. Conclusions and Future Work

It only takes two "Gunnplexer" microwave transceiver modules and a few other parts to build a low-cost SAR imaging system. From the results presented in this paper, it is clear that SAR imaging on a budget was achieved. The unique approach to FMCW radar was presented and shown to be an inexpensive and fairly precise radar solution. The unique approach to FMCW radar used in conjunction with a manually operated SAR rail was successful at producing SAR imagery using four different imaging algorithms. Two of the four algorithms demonstrated the ability to form detailed imagery using the unique approach to FMCW radar. Future work should include imagery of targets other than trihedral corner reflectors. Future work should also include implementation of this or a similar system at other research institutions or by individuals interested in SAR imaging.

7. References

1. G. L. Charvat, *A Unique Approach to Frequency-Modulated Continuous-Wave Radar Design*, MS thesis, Michigan State University, East Lansing, MI, 2003.

2. G. L. Charvat and L. C. Kempel, "Synthetic Aperture Radar Imaging Using a Unique Approach to Frequency-Modulated Continuous-Wave Radar Design," AMTA Symposium, 2005.

3. G. L. Charvat and L. C. Kempel, "A Unique Approach to Frequency-Modulated Continuous-Wave Radar Design," AMTA Symposium, 2004.

4. J. L. Eaves and E. K. Ready, *Principles of Modern Radar*, New York, Van Nostrand Reinhold Company, 1987.

5. G. W. Stimson, *Introduction to Airborne Radar*, El Segundo, California, Hughes Aircraft Company, 1983.

6. M. Soumekh, *Synthetic Aperture Radar Signal Processing With MATLAB Algorithms*, New York, John Wiley & Sons, Inc., 1999.

7. W. G. Carrara, R. S. Goodman, and R. M. Majewski, *Spotlight Synthetic Aperture Radar Signal Processing Algorithms*, Norwood, MA, Artech House, 1995.

Report on AMTA 2005

The 2005 Antenna Measurements Techniques Association (AMTA) Annual Meeting and Symposium was held at the Newport Marriott Hotel in Newport, Rhode Island, from October 30 to November 4, 2005. The hotel was ideally located at the Newport harbor (Figure 1), where there were many beautiful and historic sites to see within walking distance.

The Sunday short course in 2005 was "From Sanguine to Seafarer to ELF Communications," taught by Dr. Don Miller and Ed Wolkoff (Figure 2). This full-day course covered the thirty-year development of the Navy's extremely-low-frequency (ELF) communications system. The enthusiastic presenters provided a wealth of historic and technical information on this subject that would be difficult to find anywhere else.

On Tuesday night, there was a guest lecture, "Broadband Over Power Lines," provided by Ed Hare, the manager of the ARRL Laboratory in Newington, CT (Figures 3, 4). The Tuesday-night guest lecture instigated insightful discussion on this topic.

The Technical Program Committee, headed by Dr. Randy Jost, organized an excellent technical program, with 100 papers published in the *Proceedings*. The best paper in each session was chosen by the Technical Review Committee during the symposium, and the top six Best Papers of 2005 AMTA will be presented through the "AMTA Corner" column over the upcoming year. In addition, the *AMTA Newsletter* will present additional Best Papers from the 2005 Symposium throughout 2006. Of the 100 papers presented at the symposium, twelve papers were authored by students. Three of the twelve student papers were presented with student paper awards, as selected by the Student Paper Technical Review Committee. One of the student awards was from a US institution, and two of the student awards were from European institutions. Many of their presentations were the equal of any other author at the symposium, which bodes well for the future of the antenna measurement field and for AMTA. In fact, three of the student papers were selected as Best Papers for their session by the Technical Review Committee.

The symposium featured 16 technical sessions, which spanned a wide range of measurement topics, including "Range Design and Evaluation Topics," "Compact Range Measurement

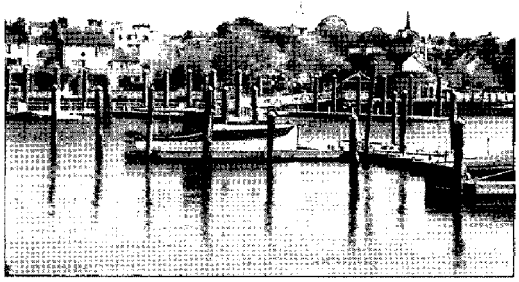

Figure 1. The Newport harbor, Newport, Rhode Island, where the AMTA 2005 meeting was held.

Figure 2. The Sunday short course, "From Sanguine to Seafarer to ELF Communications."